

1 **Depth drives the distribution of microbial ecological functions in the coastal western**
2 **Antarctic Peninsula**

3 Avishek Dutta^{1,2,3*}, Elizabeth Connors¹, Rebecca Trinh⁴, Natalia Erazo¹, Srishti Dasarathy¹,
4 Hugh W. Ducklow⁴, Deborah K. Steinberg⁵, Oscar M. Schofield⁶, Jeff S. Bowman^{1,7}

5 ¹Integrative Oceanography Division, Scripps Institution of Oceanography, UC San Diego, La
6 Jolla, CA 92093, USA

7 ²Department of Geology, University of Georgia, Athens, GA 30602, USA

8 ³Savannah River Ecology Laboratory, University of Georgia, Aiken, SC 29808, USA

9 ⁴Department of Earth and Environmental Sciences, Lamont-Doherty Earth Observatory,
10 Columbia University, Palisades, NY 10964, USA

11 ⁵Department of Biological Science, Virginia Institute of Marine Science, William & Mary,
12 Gloucester Point, VA 23062, USA

13 ⁶Department of Marine and Coastal Sciences, Rutgers University, New Brunswick, NJ 08901,
14 USA

15 ⁷Center for Microbiome Innovation, UC San Diego, La Jolla, CA 92093, USA

16 **Corresponding Author:**

17 Avishek Dutta

18 E-mail ID: avishek.dutta@uga.edu

19 **Abstract**

20 The Antarctic marine environment is a dynamic ecosystem where microorganisms play an
21 important role in key biogeochemical cycles. Despite the role that microbes play in this ecosystem,
22 little is known about the genetic and metabolic diversity of Antarctic marine microbes. In this
23 study we leveraged DNA samples collected by the Palmer Long Term Ecological Research
24 (LTER) project to sequence shotgun metagenomes from 48 key locations across the marine
25 ecosystem of the western Antarctic Peninsula. We developed an *in silico* metagenomics pipeline
26 (iMAGine) for processing metagenomic data and constructing metagenome-assembled genomes
27 (MAGs), identifying a diverse genomic repertoire related to the carbon, sulfur, and nitrogen cycles.
28 A novel analytical approach based on gene coverage was used to understand the differences in
29 microbial community functions across depth and region. Our results showed that microbial
30 community functions were partitioned based on depth. Bacterial members harbored diverse genes
31 for carbohydrate transformation, indicating the availability of processes to convert complex

32 carbons into simpler bioavailable forms. We generated 137 dereplicated MAGs giving us a new
33 perspective on the role of prokaryotes in the coastal western Antarctic Peninsula. In particular, the
34 presence of autotrophic prokaryotes capable of autotrophic and heterotrophic lifestyles indicated
35 a metabolically flexible community, which we hypothesize enables survival under rapidly
36 changing conditions. Overall, the study identified key microbial community functions and created
37 a valuable sequence library collection for future Antarctic genomics research.

38 **1. Introduction**

39 Marine microorganisms play an important role in regulating biogeochemical cycles (Green et al.,
40 2008). They are key drivers of the transformation of carbon-, nitrogen-, and sulfur-containing
41 compounds in the environment. Changes in environmental conditions impact microbial
42 communities, which in turn exert control over many environmental parameters (Thompson et al.,
43 2017; Dutta et al., 2022). The ecological outcomes of the rapid environmental change are well
44 documented for the western Antarctic Peninsula (wAP) (Meredith and King, 2005; Clarke et al.,
45 2007; Bowman et al., 2016, 2017), home to multiple long-term observing programs. Large shifts
46 in bacterial production relative to primary production signal radically different outcomes for
47 primary production from one year to another (Bowman et al., 2016). The metabolic potential of
48 the heterotrophic bacterial community is presumed to play a strong role in determining what
49 primary production gets recycled by the microbial food web. However, we know little about the
50 genomic makeup of the bacteria and archaea responsible for bacterial production and other marine
51 microbial processes along the wAP (Bowman et al., 2018).

52 Heterotrophic bacterial populations are intimately linked to phytoplankton blooms and play an
53 essential role in the transformation of phytoplankton-derived organic matter (Buchan et al., 2014).
54 Phytoplankton are a direct source of dissolved organic carbon (DOC) for heterotrophic bacteria in
55 the photic zone. Below the photic zone, heterotrophs reprocess DOC and degrade sinking particles
56 to generate new DOC. The timing of the seasonal phytoplankton bloom, its composition, and its
57 intensity are strongly influenced by physical processes along the wAP. For example, conditions
58 that favor large diatoms are thought to transfer carbon more efficiently to krill and upper trophic-
59 level consumers (Saba et al., 2014). Alternatively, strong winds and reduced sea ice cover can lead
60 to lower levels of primary production and smaller phytoplankton cells, in turn leading to high rates
61 of bacterial production compared to primary production (Bowman et al., 2016). Recent trends and

62 future climate scenarios suggest an increase in wind and a reduction in sea ice for the Antarctic
63 peninsula (Siegert et al., 2019) and, presumably, a strengthened microbial food web. To better
64 understand the metabolic capabilities of wAP marine bacterial communities, we applied
65 metagenomics to a historic sample library of microbial DNA collected by the Palmer Long Term
66 Ecological Research (LTER) project to better understand how bacterial communities will respond
67 to future environmental change along the wAP.

68 Most primary production along the wAP is attributed to eukaryotic phytoplankton (Schofield et
69 al., 2018; Lin et al., 2021). However, dark carbon fixation is likely to be a significant process
70 below the photic zone and during the polar night. Though well appreciated for the global ocean
71 (Baltar and Herndl, 2019), surprisingly little is known about the distribution of prokaryotic carbon
72 fixation mechanisms in the Antarctic marine environment. Previous analysis of fosmid libraries
73 from contrasting summer and winter communities along the wAP identified gammaproteobacterial
74 sulfur-oxidizing (GSO) chemolithotrophs (Grzymski et al., 2012). Other works using 16S rRNA
75 gene surveys have shown these taxa to be widely distributed in the coastal Antarctic (Bowman and
76 Deming, 2017; Bowman et al., 2017). Alternate prokaryotic carbon fixation strategies for the wAP
77 may rely on energy obtained from nitrification (Bowman et al., 2016). **This study aimed to**
78 **understand the microbial community functions in the marine ecosystem of coastal wAP.** We
79 applied a novel analytical approach based on the gene coverage to investigate the distribution of
80 genes and reconstructed metagenome-assembled genomes (MAGs) to understand the pathways
81 associated with prokaryotic carbon fixation and utilization. We combined observations of genes
82 diagnostic of carbon fixation with genes for catabolic processes to identify autotrophic,
83 mixotrophic, and heterotrophic guilds among wAP marine prokaryotes.

84 **2. Methods**

85 ***2.1. Sample collection***

86 Forty-eight samples were selected covering different depth horizons (0-275 m) on the Palmer
87 LTER sampling grid (lines 100-600, covering latitudes 67.566533 °S to 63.96565 °S) (Waters and
88 Smith, 1992) and locations of special significance such as Palmer Canyon, Armstrong Reef, and
89 the coastal LTER time-series near Palmer Station (Figure 1). The selection of samples was made
90 based on three different parameters: (i) higher abundances of unclassified taxa based on 16S rRNA
91 amplicon sequence data, (ii) depth profile, and (iii) variations in latitude. A detailed description of

92 the samples used in this study is given in Supplementary Table S1. Forty-two samples were
93 collected during the austral summer of 2019-2020, and four samples were collected during the
94 austral summer of 2018-2019. The remaining two samples were collected in January 2017 and
95 November 2018. We grouped the sampled into three depth horizons: shallow (0-40 m), medium
96 (50-75 m), and deep (100-275 m). The depth categorization was done based on mixed layer depth,
97 temperature, and salinity as reported previously in Schofield et al., 2018 and Seyitmuhammedov
98 et al., 2022. There were 23 samples collected from the shallower depth, whereas 11 and 14 samples
99 were collected from the medium-depth and deeper horizons, respectively. The samples were also
100 categorized into three regions based on Palmer LTER lines: Northern (Line 400 and north of Line
101 400), Southern (south of Line 400), and Palmer Canyon (near Palmer Station on Anvers Island)
102 (Supplementary Table S1). There were 14 samples collected from the Northern region, whereas
103 16 and 18 samples were collected from Palmer Canyon and the Southern region, respectively. For
104 each sample, approximately 1 L of seawater was filtered through a sterile 0.2 μ m Supor membrane
105 disc filter (Pall Corporation, Port Washington, NY, USA) and stored at -80 °C until extraction.

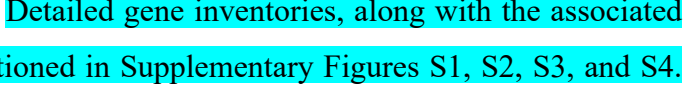
106 **2.2.DNA extraction, sequencing, and metagenome analysis**

107 DNA was extracted from the filters using the MagMAX Microbiome Ultra nucleic acid extraction
108 kit and KingFisher Flex extraction system following the manufacturer's protocols. The extracted
109 DNA was sequenced at the UC San Diego Microbiome Core for shotgun metagenome sequencing
110 on the Illumina NovaSeq platform. Sequencing was done across multiple lanes in two runs (24
111 samples for each run). The average depth of sequencing for the second run (an average of ~427
112 million paired-end reads per sample) was higher compared to the first run (an average of ~55
113 million paired-end reads per sample) to facilitate a separate analysis that will be reported
114 elsewhere. To avoid memory limitation, samples from the second run were down-sampled using
115 reformat.sh, a script from the BBMap package (Bushnell, 2014), to ~55 million paired-end reads
116 per sample. The raw metagenomic data for 48 samples were processed and analyzed using the *in*
117 *silico* Metagenomics Pipeline (iMAGine) using default parameters
118 (<https://github.com/avishekdutta14/iMAGine>). iMAGine uses fastp (Chen et al., 2018) for
119 filtering, metaSPAdes (Nurk et al., 2017) for assembling the reads, QUAST (Gurevich et al., 2013)
120 for analyzing the assembly quality, bwa-mem (v0.7.17) for aligning the raw reads to the assembly
121 (Li, 2013), samtools for modifying alignment files (Li et al., 2009), metabat2 (Kang et al., 2019)

122 for binning contigs, and checkM (Parks et al., 2015) for quality assessment of the bins. The
123 assembled contigs from iMAGine were used for further analyses.

124 Genes were predicted from contigs with Prodigal v2.6.3 (Hyatt et al., 2010) using the ‘meta’ flag.
125 The predicted genes were annotated using emapper v2.1.5 (Cantalapiedra et al., 2021) based on a
126 Diamond search (Buchfink et al., 2014). The following arguments were used for search filtering
127 in emapper: --evaluate 0.001 (e-value threshold), --score 60 (minimum hit bit score), --pident 40
128 (minimum percentage identity), --query_cover 20 (minimum percentage query coverage), and --
129 subject_cover 20 (minimum percentage subject coverage). The database used for annotation was
130 eggNOG DB v5.0.2 (Huerta-Cepas et al., 2019).  In this study, taxfin.sh (a part of iMAGine) was
131 used for keeping genes affiliated to domain bacteria and archaea. Coverage of each gene (average
132 gene fold) was determined using gene_fold_counter.sh (a part of iMAGine), which takes in the
133 alignment map file (sam output from iMAGine), removes unmapped reads and reads mapped to
134 multiple locations using samtools (with parameters -F 0x904), uses pileup.sh script from the
135 BBMap package to calculate the average coverage of the contigs and maps back average contig
136 coverage to the genes on those contigs. To enable comparison across metagenomes, all the genes
137 were scaled based on Eqt 1:

138
$$\text{Normalized gene coverage of a sample} = \frac{\text{Total average gene coverage}}{\text{Total } rpoB \text{ (K03043) coverage}} \quad (1)$$

139 For gene-specific analysis, KEGG orthologs from the emapper outputs were considered. Genes
140 mapping to more than one ortholog were not considered for the analysis. Key genes involved in
141 different processes of carbon, nitrogen, and sulfur cycles were selected based on KEGG pathways,
142 whereas genes involved in carbohydrate transformation were selected based on previously
143 published literature (Bergauer et al., 2018).  Detailed gene inventories, along with the associated
144 pathways considered in this study, are mentioned in Supplementary Figures S1, S2, S3, and S4.
145 The KEGG ortholog for *rpoB* i.e. K03043 was used as a reference for normalization in this study.
146 The genes involved in methane oxidation considered in this study (*pmoA-amoA*, *pmoB-amoB*, and
147 *pmoC-amoC*) also play an important role in ammonia oxidation (a key step in nitrification).
148 Similarly, it has been seen before that the variations of the same gene responsible for dissimilatory
149 sulfate reduction (considered in this study) are also involved in sulfur oxidation (Loy et al., 2009).

150 Bins with completeness higher than 70% and contamination lower than 5% were considered
151 MAGs. Similar cutoffs were used in a previous study (Parks et al., 2017). For further analysis,
152 MAGs were dereplicated with dRep v3.2.2 (Olm et al., 2017) using a secondary ANI threshold of
153 0.96 and goANI as the algorithm for secondary clustering. The minimum genome completeness
154 was set to 70%, and the maximum genome contamination was set to 5% for dereplication. All the
155 other dereplication parameters were kept default. The taxonomy of the dereplicated MAGs was
156 assessed using the GTDB-Tk v1.5.0 based on reference database version release 202 (Chaumeil et
157 al., 2020). The multiple sequence alignment output of domain-specific marker genes from GTDB-
158 Tk was used for constructing a phylogenomic tree with RAxML-ng (Kozlov et al., 2019). Tree
159 construction used the WAG amino-acid substitution model and MAGs belonging to Chloroflexota
160 and Thermoproteota as outgroups for bacteria- and archaea-specific phylogenomic trees,
161 respectively. The default number of starting trees was used (ten random and ten parsimony-based)
162 and one thousand bootstrap replicates were used for confidence scoring of the final tree.

163 The number of reads mapped to each MAG was calculated using the mag_abund.py script present
164 in the iMAGine repository
165 (https://github.com/avishhekuttal4/iMAGine/blob/main/Utilities/mag_abund.py), and the
166 average reads per secondary cluster (as obtained from dRep analyses) was obtained to understand
167 average reads mapped per dereplicated MAGs.

168 ***2.3. Determination of putative metabolic lifestyle in MAGs***

169 Functional annotation of MAGs was conducted using two different methods. To identify functional
170 guilds, genes were predicted using Prodigal v2.6.3 and annotated using Ghost Koala (Kanehisa et
171 al., 2016), whereas DRAM 1.4.0 was used to assess pathway completeness and categorize different
172 microbial metabolisms (Shaffer et al., 2020). Though it is hard to ascertain the exact metabolic
173 lifestyle of the MAGs given the limitation imposed by genome completeness, we described the
174 putative metabolisms based on combinations of diagnostic metabolic pathways. All the
175 annotations for metabolic lifestyle assessment were based on DRAM analysis. Glucose utilization
176 (GU) and carbon fixation (CF) pathways having greater than 70% completeness in a MAG were
177 considered in this study. GU, indicative of the use of exogenous fixed carbon, was assessed by the
178 presence of the Embden Meyerhof pathway and/or the Entner-Doudoroff pathway. CF was
179 assessed based on the presence of either of the three carbon fixing pathways (3-Hydroxypropionate

180 bicycle, Arnon–Buchanan cycle, and Calvin cycle) found in the MAGs. Sulfur oxidation (SO)
181 capability was determined based on the presence of the SOX system and/or the presence of the *dsr*
182 gene. Nitrification (NI) capability was determined based on the presence of either ammonia
183 oxidation genomic repertoire and/or gene involved in the conversion of nitrite to nitrate.
184 Denitrification (DNR) capability was determined based on the presence of either one of the genes
185 involved in the following processes: (i) genes involved in the conversion of nitrate to nitrite, (ii)
186 genes involved in the conversion of nitrite to nitric oxide, and/or (iii) genes involved in the
187 conversion of nitric oxide to nitrous oxide. We described each MAG as a putative autotroph,
188 mixotroph, or heterotroph based on the presence of diagnostic metabolic pathways. Autotrophs
189 were determined by the presence of CF and absence of GU, heterotrophs by the presence of GU
190 and absence of CF, and mixotrophs by the presence of both GU and CF.

191 **2.4. Statistical analyses**

192 All the statistical analyses were carried out in R and R Studio (Team, 2015). Principal Coordinates
193 Analysis (PCoA) of Bray-Curtis dissimilarity based on the normalized gene coverage across
194 different samples was performed using the phyloseq package (McMurdie and Holmes, 2013). For
195 this PCoA, we considered key genes responsible for carbon, nitrogen, sulfur, and carbohydrate
196 transformations (Supplementary Figure S1, S2, S3, S4). A PERMANOVA test was conducted
197 using the ‘adonis2’ function of the Vegan package (Oksanen et al., 2007) to test whether different
198 sample groups had different centroids. The average distance from the median was calculated based
199 on a dispersion test using the ‘betadisper’ function of the Vegan package, which was followed by
200 a permutation test of multivariate homogeneity of group dispersions using the ‘permute’ function
201 of the Vegan package. Boxplots were made to analyze the differences in process abundances across
202 different depth profiles. The Kruskal-Wallis test for significance was used to determine whether
203 the overall changes were significant, whereas the Wilcoxon test was used to find the pairwise
204 significance. Heatmap and cluster analyses were carried out with the pheatmap package (Kolde,
205 2019) and based on normalized gene coverage. Column clustering, which displayed the clustering
206 of different samples, was based on Bray–Curtis dissimilarity. Each row, depicting normalized
207 gene coverage, was scaled using min-max scaling and clustered based on correlation. To
208 understand the clustering of MAGs based on genomic repertoire, genes obtained from Ghost Koala
209 analysis were mapped to each dereplicated MAGs using custom R scripts, and Non-Metric

210 Multidimensional Scaling (NMDS) of a binary matrix based on the presence or absence of all
211 genes constraining different metabolic categories were performed using Vegan. All the statistical
212 analyses for the MAGs were conducted based on dereplicated MAGs, except for the mapped read
213 coverage analysis. For mapped read coverage, all the MAGs were considered. A web-based tool
214 (<https://bioinformatics.psb.ugent.be/webtools/Venn/>) was used to generate Venn diagrams to find
215 the overlap across different metabolic categories to determine metabolic lifestyle of the MAGs.

216 **3. Results**

217 ***3.1. Microbial community function***

218 Microbial community functions varied across depths (Figure 2). Three distinct clusters were
219 observed for deep, medium-deep, and shallow samples with minor overlaps based on normalized
220 gene coverage (PERMANOVA, $p = 0.001$). One of the medium-deep samples (Armstrong Reef)
221 clustered with the shallower-depth samples. Dispersion among sample groups differed according
222 to depth ($p = 0.001$). The average distance from the median was highest for shallower depth
223 samples, followed by medium-deep and deeper samples. The samples were also significantly
224 different (PERMANOVA, $p = 0.011$) based on region (Southern, Northern, and Palmer Canyon).
225 However, the separation of samples was more pronounced for depth than region according to the
226 PERMANOVA F-ratio ( $F_h = 10.224$, and $F_{region} = 2.6985$). We conducted a detailed study of
227 carbon, nitrogen, sulfur, and carbohydrate metabolism-specific genes based on normalized gene
228 coverage to understand the differential abundances of functional genes across different depth
229 horizons and regions.

230 ***3.1.1. Carbon cycle***

231  genes involved in prokaryotic dark carbon fixation, carbon monoxide oxidation, fermentation,
232 methane oxidation, and photoheterotrophy were explored to understand carbon transformation and
233 their distribution in the wAP. Varied abundances of groups of genes involved in different carbon
234 transformation processes were observed across different depths (Supplementary Figure S1). Genes
235 associated with dark carbon fixation were found to be significantly higher in the deeper samples
236 compared to medium-depth ($p = 9 \times 10^{-7}$) and shallower samples ($p = 0.00085$) (Figure 3A). The
237 abundance of the genes involved in CO oxidation varied across depths. The deeper samples
238 harbored significantly greater CO oxidation gene coverages compared to shallower ($p = 0.00096$)

239 and medium-deep samples ($p = 4.4 \times 10^{-5}$) (Figure 3B). A similar trend was observed for genes
240 involved in fermentation and methane metabolism (Figures 3C and 3D).

241 **3.1.2. *Sulfur cycle***

242 The abundance of genes involved in the oxidation and reduction of sulfur species varied across
243 depths (Supplementary Figure S2). Normalized coverages of genes involved in sulfur oxidation
244 were found to be significantly higher in the shallower samples compared to medium-depth ($p =$
245 0.0051) and deeper samples ($p = 3.9 \times 10^{-5}$) (Figure 4A). On the contrary, normalized coverage of
246 genes involved in dissimilatory sulfate reduction were found to be significantly higher in the
247 deeper samples compared to medium-depth ($p = 9 \times 10^{-7}$) and shallower samples ($p = 6.9 \times 10^{-6}$)
248 (Figure 4B). Normalized coverage of genes involved in thiosulfate to sulfide reduction was found
249 to be the highest in the deeper samples, followed by medium-depth and shallower samples (Figure
250 4C).

251 **3.1.3. *Nitrogen cycle***

252 The abundances of the genes involved in oxidation and reduction of nitrogen species also varied
253 with depth (Supplementary Figure S3). The average coverages of the genes involved in
254 nitrification were significantly higher in the deeper horizons of the water column compared to
255 medium-depth ($p = 0.0051$) and shallower horizons ($p = 4.1 \times 10^{-7}$) (Figure 5A). Similarly, the
256 abundance of genes involved in denitrification and dissimilatory nitrate reduction to ammonia
257 (DNRA) was found to be significantly higher in deeper samples compared to medium-deep
258 (Denitrification: $p = 5.4 \times 10^{-6}$; DNRA: $p = 0.00012$) and shallower depth (Denitrification: $p = 3.9$
259 $\times 10^{-9}$; DNRA: $p = 0.026$) samples (Figures 5B and 5C). Genes involved in urea utilization were
260 also observed in all the wAP samples. Urea-utilizing gene coverages were found to be significantly
261 higher in the deeper horizon samples compared to samples from the medium depth ($p = 4.5 \times 10^{-7}$)
262 and shallower depth ($p = 0.00013$) horizons (Figure 5D).

263 **3.1.4. *Carbohydrate transformations***

264 We further analyzed genes involved in the transformation of glycoprotein, cellulose, chitin, pectin,
265 starch, xylans, and xyloglucans to understand the carbohydrate pool and transformation
266 capabilities of microorganisms across different depth horizons of the wAP (Supplementary Figure
267 S4). Cellulose, pectin (RGI), starch, and xyloglucans metabolizing gene coverages were found to

268 be significantly higher in the shallower depth samples compared to medium-deep (Cellulose: $p =$
269 0.00033; pectin [RGI]: $p = 8.6 \times 10^{-5}$; starch: $p = 0.0095$; and xyloglucans: $p = 0.0051$) and deeper
270 samples (cellulose: $p = 2.7 \times 10^{-5}$; pectin [RGI]: $p = 1.8 \times 10^{-6}$; starch: $p = 0.00074$; and
271 xyloglucans: $p = 2.3 \times 10^{-5}$) (Figures 6 A,B,C,D). Abundances of chitin metabolizing genes were
272 significantly higher in deeper samples compared to the samples from medium depth ($p = 8.7 \times 10^{-5}$)
273 and shallow samples ($p = 0.0029$) (Figure 6E).

274 **3.2. Distribution, taxonomy, and metabolic profiles of MAGs**

275 A total of 2940 bins were obtained from 48 samples. Of these, 612 bins with genome completeness
276 of more than 70% and contamination of less than 5% were considered MAGs and used for further
277 analysis. These 612 MAGs were filtered down to 609 MAGs by dRep based on genome quality
278 and were dereplicated to a final set of 137 MAGs. 137 MAGs (representing 609 MAGs) covered
279 13.11%, 5.96%, and 2.12% of the total filtered reads from deep, medium-deep, and shallow
280 samples, respectively (Figure 7). The most abundant MAG found in the shallower waters was
281 affiliated with Bacteroidota (represented by ANT-68) (Figure 7A). This MAG was exclusively
282 observed in the shallow environments of the coastal wAP. Among these 137 MAGs, 64 MAGs
283 were unique to deep samples, whereas 19 and 15 MAGs were unique to the medium and shallow
284 horizons, respectively. 11 MAGs were found in all three depth horizons, and the remaining 28
285 MAGs were found in two of the three horizons (medium and deep: 18, shallow and medium: 9,
286 and shallow and deep: 1). When sorted by region, 33 MAGs represented MAGs unique to the
287 Southern region, whereas 32 and 4 MAGs represented MAGs unique to the Palmer Canyon and
288 Northern region, respectively. 21 MAGs were found in all three regions, and the remaining 47
289 MAGs were found in two of the three regions (Southern – Palmer Canyon: 30, Southern –
290 Northern: 14, and Northern – Palmer Canyon: 3). The most abundant MAG found in the medium-
291 depth waters was affiliated with family SAR324 (represented by ANT-96) (Figure 7B). This MAG
292 was observed in the medium-depth and deeper samples. ANT-96 was also found to be the most
293 abundant MAG in deeper waters (Figure 7C). Considering the proportion of reads that mapped to
294 each MAG, the overall highest average mapped read percentage was also found in ANT-96 (2.11%
295 $\pm 1.22\%$; representing 7 MAGs from different samples). Detailed genome statistics of the 137
296 MAGs are present in Supplementary Table S2.

297 The MAGs were taxonomically diverse. Of 137 MAGs, 10 MAGs were affiliated with the domain
298 Archaea, and 127 MAGs were affiliated with Bacteria. Average nucleotide identity (ANI) or
299 relative evolutionary divergence (RED) values were analyzed for each MAG based on reference
300 genomes from GTDB using GTDB-Tk. RED values were calculated when the MAGs were unable
301 to be classified based on ANI. ANI values greater than 0.95 were obtained for 40 MAGs (2
302 archaeal MAGs and 38 bacterial MAGs), whereas RED values (ranging between 0.660 to 0.998)
303 were obtained for the rest of the MAGs (Supplementary Table S3). Nine of the archaeal MAGs
304 were affiliated with the phylum Thermoplasmatota whereas one was affiliated with
305 Thermoproteota (Figure 8A). Among the ten archaeal MAGs, two MAGs had formal taxonomic
306 nomenclature (as indicated in International Code of Nomenclature of Prokaryotes) at the genus level
307 (*Nitrosopumilus* and *Thalassarchaeum*), and one of the Thermoplasmatota MAGs had a separate
308 branch from the root of the phylogenomic tree. Bacterial MAGs were assigned to 13 different
309 phyla (Figure 8B). The highest number of MAGs were affiliated with Proteobacteria (53 MAGs),
310 followed by 17 and 14 MAGs affiliated with Planctomycetota and Verrucomicrobiota,
311 respectively. Out of 127 bacterial MAGs, 61, 28, and 5 MAGs had a formal taxonomic
312 nomenclature at the family, genus, and species levels, respectively. Two bacterial MAGs affiliated
313 with class Alphaproteobacteria (ANT-120) and phylum Planctomycetota (ANT-49) had RED
314 values lower than 0.70. Detailed taxonomy classifications of all 137 MAGs are present in
315 Supplementary Table S3. It was interesting to note that one of the MAGs classified as
316 Myxococcota by GTDB-Tk clustered with Proteobacterial MAGs on the phylogenomic tree
317 (Figure 8B).

318 Distinct groups of MAGs were observed when clustered according to their metabolic profiles. The
319 NMDS plot indicated that the metabolic profiles of bacterial populations were phylum-specific,
320 with minor overlaps among phyla (Figure 9). Distinct clusters for archaeal and bacterial MAGs
321 were observed on the PCoA plot based on genomic repertoire (PERMANOVA, $p = 0.001$)
322 (Supplementary Figure S5). Specific gene sets and pathways were studied to determine the
323 metabolic capabilities of the MAGs (Supplementary Table S4 and Supplementary Figure S6).

324 **3.2.1. Role of MAGs in carbon transformation**

325 Capabilities of glucose utilization and carbon fixation were analyzed based on different pathways.
326 Since these pathways have multiple enzymes involved in them, pathways having $\geq 70\%$

327 completeness in a MAG were considered as the presence of the pathway in the MAG. The details
328 of the pathways and the completeness profiles are described in Supplementary Table S4. The
329 capability to use externally fixed carbon was studied based on the presence of the Embden
330 Meyerhof and Entner–Doudoroff pathways. These two pathways help in the conversion of glucose
331 into pyruvate. 75 MAGs covering ten phyla had the capability of performing the Embden
332 Meyerhof pathway, whereas 42 MAGs covering seven phyla had genomic repertoires for the
333 Entner–Doudoroff pathway. The pentose phosphate pathway was observed in 88 MAGs covering
334 11 phyla. The citrate cycle (Krebs cycle) was observed in 112 MAGs, whereas the glyoxylate cycle
335 was observed in 40 MAGs. Three carbon fixation pathways *viz.* 3-Hydroxypropionate bicycle,
336 Arnon–Buchanan cycle (reductive citrate cycle), and Calvin cycle (reductive pentose phosphate
337 cycle) were observed among the MAGs. Capabilities of the Arnon–Buchanan cycle were present
338 in a higher number of MAGs (56 MAGs) compared to the Calvin cycle (present in 26 MAGs) and
339 3-Hydroxypropionate bicycle (present in 8 MAGs). 3-Hydroxypropionate bicycle was only
340 present in Proteobacterial MAGs, whereas Arnon–Buchanan cycle was distributed over MAGs
341 affiliated to Proteobacteria, Verrucomicrobiota, Actinobacteriota, Planctomycetota,
342 Chloroflexota, Thermoplasmatota, SAR324, and Latescibacterota. Calvin cycle was present in
343 MAGs affiliated to Proteobacteria, Actinobacteriota, Chloroflexota, Bacteroidota,
344 Planctomycetota, Gemmatimonadota, and SAR324.

345 The ability to produce or catabolize small-chain fatty acids and alcohols was studied based on the
346 presence of certain genes in the genomic inventories of the MAGs. Capabilities of alcohol
347 production (EC 1.1.1.1) were found in 53 MAGs, with the majority of the MAGs affiliated with
348 Proteobacteria. The presence of genes encoding for phosphate acetyltransferase (EC 2.3.1.8)
349 and/or acetate kinase (EC 2.7.2.1) was studied to understand acetate metabolism in the MAGs.
350 Genes encoding for acetate metabolizing enzymes were found in 21 MAGs which were affiliated
351 with six different phyla (Proteobacteria, Verrucomicrobiota, Planctomycetota, Actinobacteriota,
352 Latescibacterota, and Bacteroidota). Genes encoding for L-lactate metabolizing enzyme (L-lactate
353 dehydrogenase) were found in 19 MAGs, which were affiliated with the Proteobacteria,
354 Actinobacteriota, Verrucomicrobiota, and Planctomycetota, whereas genes encoding for D-lactate
355 metabolizing enzyme (D-lactate dehydrogenase) were found in five MAGs affiliated with
356 Proteobacteria, Verrucomicrobiota, and Bacteroidota. The gene encoding for propionate

357 metabolism (propionate CoA transferase) was found in three MAGs affiliated with two different
358 phyla (Proteobacteria and Verrucomicrobiota).

359 Genes encoding for carbohydrate-active enzymes were studied to understand the polysaccharide-
360 degrading capabilities of the MAGs. Genes encoding for enzymes involved in breaking down
361 amorphous cellulose were found in 30 MAGs affiliated with seven different phyla (Proteobacteria,
362 Planctomycetota, Bacteroidota, Myxococcota, Verrucomicrobiota, Actinobacteriota, and
363 Latescibacterota), whereas genes encoding for the enzyme involved in breaking down crystalline
364 cellulose was found in 11 MAGs covering five phyla (Planctomycetota, Proteobacteria,
365 Verrucomicrobiota, Actinobacteriota, and Myxococcota). Genes coding for chitin-degrading
366 enzymes were found in 85 MAGs (found in all phyla detected in this study except for MAGs
367 affiliated with Thermoproteota, Chloroflexota, and Thermoplasmatota), whereas genes for starch-
368 degrading enzymes were found in 15 MAGs having affiliation with five phyla (Proteobacteria,
369 Verrucomicrobiota, Planctomycetota, Actinobacteriota, and Latescibacterota). Genes encoding
370 enzymes that can perform Xylan and xyloglucan (major components of hemicellulose) degradation
371 were found in 23 and 40 MAGs, respectively. MAGs with the ability to degrade xylan were
372 affiliated with Proteobacteria, Bacteroidota, Myxococcota, Planctomycetota, Actinobacteriota,
373 and Latescibacterota, whereas MAGs with the ability to degrade xyloglucan were affiliated to
374 Proteobacteria, Bacteroidota, Verrucomicrobiota, Planctomycetota, Myxococcota,
375 Latescibacterota, and Marinisomatota. Genes encoding pectin degradation enzymes were found in
376 31 MAGs (having affiliation with Proteobacteria, Verrucomicrobiota, Planctomycetota,
377 Bacteroidota, Latescibacterota, Marinisomatota, Gemmatimonadota, Acidobacteriota, and
378 Chloroflexota).

379 ***3.2.2. Role of MAGs in sulfur and nitrogen transformation***

380 Genes involved in thiosulfate oxidation were found in 26 MAGs having affiliations with five phyla
381 (Proteobacteria, Gemmatimonadota, Acidobacteriota, and SAR324) (Supplementary Figure S6).
382 Three proteobacterial MAGs were found to harbor genes for dissimilatory sulfate reduction.

383 Genes involved in ammonia oxidation were found in two proteobacterial MAGs and in one
384 archaeal MAG (affiliated to Thermoproteota). Genes involved in the conversion of nitrite to nitrate
385 (one of the steps in nitrification) were found in two proteobacterial MAGs. Genes involved in the
386 conversion of nitrate to nitrite (one of the steps in denitrification or dissimilatory nitrate reduction

387 to ammonia) were found in two proteobacterial MAGs. Enzymes involved in the conversion of
388 nitrite to nitric oxide (a key step in denitrification) were found in 14 different MAGs covering
389 eight phyla (Proteobacteria, Actinobacteriota, Thermoproteota, Gemmatimonadota,
390 Verrucomicrobiota, Acidobacteriota, Bacteroidota, and Nitrospinota), whereas enzymes involved
391 in the conversion of nitric oxide to nitrous oxide (an additional step in denitrification) were found
392 in two proteobacterial MAGs.

393 **3.3. Putative metabolic lifestyles of MAGs**

394 Overlaps across these categories are reported in Figures 8 and 10A. It was found that the average
395 genome sizes of the mixotrophs were significantly higher compared to heterotrophs ($p = 0.0001$)
396 and autotrophs ($p = 0.02$) (Figure 10B). In the shallower depth samples, a significantly high
397 mapped read percentage was observed in the mixotrophic MAGs ($n = 37$ MAGs), while compared
398 to the autotrophic ($n = 2$ MAGs) and heterotrophic MAGs ($n = 52$ MAGs) (mixotroph vs.
399 autotrophs, $p = 0.054$; mixotroph vs. heterotroph, $p = 1.5 \times 10^{-5}$) (Figure 10C). In the medium and
400 deeper samples, the mapped read percentages for mixotrophic, autotrophic, and heterotrophic
401 MAGs were not significantly different.

402 **3.3.1. Putative mixotrophs**

403 Four categories of mixotrophs covering 52 dereplicated MAGs were obtained (Supplementary
404 Figure S6 and Supplementary Table S4). Only one MAG (ANT-6) recovered from a deeper
405 horizon sample and classified as *Paraburkholderia* was found to harbor genes from all four
406 categories of metabolism (GU, CF, SO, and NI). There were 12 MAGs that harbored genes from
407 GU, CF, and SO (11 affiliated to Proteobacteria and one affiliated to Gemmatimonadota), whereas
408 there was only one MAG that harbored genes from GU, CF, and NI (affiliated to Proteobacteria).
409 There were 38 MAGs that harbored the genes from GU and CF metabolism categories only
410 (affiliated to Proteobacteria, Actinobacteriota, Verrucomicrobiota, Planctomycetota,
411 Chloroflexota, Bacteroidota, Latescibacterota, and SAR324).

412 **3.3.2. Putative autotrophs**

413 Three categories of autotrophs covering 20 dereplicated MAGs were obtained (Supplementary
414 Table S4). There were three MAGs harboring genes for CF and SO (affiliated with
415 Gammaproteobacteria), whereas there was only one MAG harboring gene for CF and NI (affiliated

416 with Gammaproteobacteria). There were 16 MAGs that had genomic repertoire for CF but lacked
417 genes for SO and NI (affiliated with Proteobacteria, Thermoplasmatota, Planctomycetota,
418 Chloroflexota, Actinobacteriota, and Verrucomicrobiota).

419 **3.3.3. *Putative heterotrophs***

420 Two categories of heterotrophs covering 35 dereplicated MAGs were observed in this study
421 (Supplementary Figure S6 and Supplementary Table S4). One of the categories harbored genes for
422 GU and SO, which was found in five different MAGs (affiliated to Proteobacteria and SAR324).
423 The other category solely harbored genes for GU and was found in 30 MAGs (affiliated to
424 Proteobacteria, Bacteroidota, Verrucomicrobiota, Planctomycetota, Actinobacteriota, SAR324,
425 and Myxococcota).

426 **4. Discussion**

427 Our analysis reveals the diverse genomic repertoire contained among marine bacteria and archaea
428 along the coastal wAP. PCoA based on normalized gene coverage across 48 samples suggested
429 that microbial community functions were strongly partitioned by depth, with the highest variation
430 in microbial community function observed in the shallower samples (0-40 m). A possible
431 explanation is that this higher variance results from a more dynamic environment in the shallower
432 waters than in the deeper environments.

433 Primary production in the coastal Antarctic is attributed primarily to phytoplankton (Arrigo et al.,
434 2008). However, prokaryotic dark carbon fixation can be significant in deep and polar oceans
435 (Alonso-Sáez et al., 2010; Williams et al., 2012; Connelly et al., 2014), and previous work has
436 identified the genomic signatures of dark carbon fixation along the wAP (Grzymski et al., 2012).
437 We observed genes indicative of dark carbon fixation in numerous MAGs representing multiple
438 phyla. This suggests that in addition to eukaryotic carbon fixation, prokaryotic dark carbon fixation
439 can also be a source of fixed carbon in the Antarctic marine ecosystem,  and the conventional
440 viewpoint of marine primary production (Buchan et al., 2014). We are not aware of any studies
441 that attempt to quantify dark carbon fixation inputs to coastal Antarctic ecosystems. However,
442 previous work suggests oceanic primary production estimates would increase by 5 %–22 % when
443 total dark dissolved organic carbon fixation is included (Baltar and Herndl, 2019). Moreover, the
444 normalized coverage of genes related to dark carbon fixation was found to be higher in deeper

445 waters compared to the waters from medium-deep and shallower horizons in the coastal wAP
446 suggesting that the dearth of phytoplankton-fixed carbon in the deeper waters selects for
447 microorganisms capable of fixing carbon in the dark. This lack of photosynthate as an electron
448 donor in deeper water is further supported by the presence of higher normalized gene coverage of
449 CO oxidation genes. Lappan et al. (2023) previously reported an enrichment of CO hydrogenase
450 (an enzyme involved in CO oxidation) in temperate mesopelagic waters and suggested that CO
451 oxidation is favored in energy-limited waters at depths where primary production is low.

452 The normalized gene coverages for processes preferred in hypoxic/anoxic environments, such as
453 fermentation, dissimilatory sulfate reduction, thiosulfate to sulfide reduction, denitrification, and
454 DNRA, were found to be higher in the water samples from the deeper horizons (>100 m).  Although
455 oxygen drawdown is observed below the photic zone in the wAP (Cape et al., 2019), the water
456 column typically remains sufficiently oxic to support aerobic processes, including nitrification and
457 methane oxidation in deeper waters. We suggest two explanations for the presence of anaerobic
458 pathways here. First, the organisms harboring these pathways may be facultative anaerobes that
459 can dwell in multiple environments of the wAP. This is supported by the presence of certain MAGs
460 capable of using oxygen (presence of cytochrome c oxidase and F-Type ATPases genes) and
461 nitrate (presence of genes involved in denitrification) as terminal electron acceptors. Second, these
462 microbial populations may come from fecal pellets and sinking detritus that harbor
463 microenvironments that support the growth of anaerobic microbial populations.

464 Due to high levels of primary production, the coastal wAP harbors a diverse and abundant
465 carbohydrate pool. The source of these carbohydrates includes phytoplankton or zooplankton such
466 as  (Oijen et al., 2003; Yu et al., 2020). We observed a diverse genomic repertoire for
467 degrading carbohydrates derived from phytoplankton and zooplankton. This suggests a link
468 between the microeukaryotic and prokaryotic populations in the Antarctic. Moreover, higher
469 abundances of microorganisms capable of degrading cellulose, xyloglucans, pectin, and starch
470 were observed in the upper water column, consistent with the greater phytoplankton biomass
471 expected there. This distribution suggests that carbohydrates are readily turned over in the upper
472 water column, possibly reducing vertical export. This is further supported by the presence of
473 prokaryotic dark carbon fixing pathways in the deeper environment of coastal wAP. Several
474 MAGs having the capability to degrade polysaccharide was also observed in the medium-deep and

475 deeper horizon of the wAP. This suggests that these microbial populations may be associated with
476 the sinking detritus material, which helps in the conversion of complex carbohydrates to simpler
477 carbon compounds that can be used by other heterotrophs.

478 Varied metabolic flexibility was observed in several MAGs. ANT-6, affiliated to
479 *Paraburkholderia fungorum* was found to have the most diverse genomic repertoire based on the
480 presence of heterotrophic and autotrophic pathways. The genomic repertoire suggests that they can
481 perform carbon fixation and also utilize glucose. The mixotrophic behavior of *Paraburkholderia*
482 has been reported previously (Herpell et al., 2020). Interestingly, ANT-6 also harbored genes
483 involved in thiosulfate oxidation, nitrification, and denitrification. Sulfite oxidation was previously
484 observed in *Paraburkholderia caledonica* PHRS4 (BioCyc ID: PWY-5276). Even though varied
485 metabolic traits of the genus *Paraburkholderia* are well known, the presence of genomic
486 machinery related to autotrophic and heterotrophic lifestyle, along with the presence of thiosulfate
487 oxidation, nitrification, and denitrification capability in a single strain, is not reported elsewhere
488 to the best of our knowledge. The genome size of ANT-6 was found to be the highest (9.3 Mbp)
489 among all the other MAGs constructed. The genome size of ANT-6 is in the range of genome sizes
490 of other *Paraburkholderia* strains (Wang et al., 2021), which is bigger than “typical” bacterial
491 genomes (Land et al., 2015). The metabolic flexibility of *Paraburkholderia* is consistent with its
492 bigger genomes size. Previous reports of the presence of *Paraburkholderia* in the Antarctic
493 environment (Malard et al., 2022) also support the presence of ANT-6 in the Antarctic.

494 A high number of mixotrophic MAGs (52 MAGs) were observed compared to exclusively
495 heterotrophic (35) and autotrophic (20) MAGs. The prevalence of mixotrophy was also previously
496 reported in Arctic prokaryotic genomes (Royo-Llonch et al., 2021). In the shallow samples of the
497 coastal wAP, the abundances of mixotrophic MAGs were found to be significantly higher
498 compared to heterotrophic and autotrophic MAGs, whereas, in the deeper samples, the abundances
499 of the mixotrophic MAGs were not significantly different compared to autotrophic and
500 heterotrophic MAGs. This suggests a strong pressure for metabolic flexibility, potentially a
501 response to the seasonal boom-bust cycle of photosynthetic primary production. This is in line
502 with the higher variations of genomic repertoire in the shallower samples compared to medium-
503 depth and deeper samples. We hypothesize that dynamic environments select microbial
504 populations with a diverse genomic repertoire, including the capacity to switch between

505 heterotrophic and autotrophic lifestyles. Moreover, the genome size of the mixotrophs was found
506 to be significantly larger compared to the autotrophs and heterotrophs. This is in accordance with
507 a previous study where they reported larger genome sizes of the generalist compared to the
508 specialist (Sriswasdi et al., 2017). However, it should be taken into account that higher
509 completeness of MAGs is required to ascertain a particular function or metabolic lifestyle with
510 greater confidence.

511 Several of our MAGs were only distantly related to the genomes of type strains. A MAG classified
512 as Myxococcota (MAG name here) by GTDB-Tk clustered with Proteobacterial MAGs on the
513 phylogenomic tree (Figure 8B) which might be due to its novel taxonomy. There might also be two
514 other reasons for this: (i) lower completeness of the Myxococcota genome (75.54 % completeness)
515 and/or (ii) close relatedness of Myxococcota genome with Proteobacterial genomes, which can be
516 supported by recent classification of Myxococcota as a new separate phylum, which was earlier
517 assigned to class Deltaproteobacteria (Murphy et al., 2021). Only 40 MAGs had ANI values higher
518 than 0.95 when compared to the genomes from the GTDB reference database. Based on our current
519 analyses, we found that only 70, 30, and 5 MAGs had a formal taxonomic nomenclature at the
520 family, genus, and species levels, respectively. We were unable to determine the metabolic
521 lifestyle of the MAG (ANT-120, affiliated to Alphaproteobacteria) having the lowest RED value
522 (0.66). Similarly, there were 29 other MAGs for which we were unable to determine the metabolic
523 lifestyle based on the criteria we used in this study.  Although this might be a limitation imposed by
524 genome completeness, there are chances of the presence of novel metabolic pathways in them.

525 This study used high-throughput metagenomics to understand the microbial role in the marine
526 ecosystem of the wAP. A streamlined metagenomic sequence analysis pipeline (iMAGine) was
527 developed to process data and reconstruct MAGs. Our pipeline enabled a coverage-based approach
528 to understand how genes were partitioned by depth and region. With this approach, we identified
529 diverse groups of microorganisms contributing to the carbon, sulfur, and nitrogen cycle along the
530 coastal wAP. Distinct microbial metabolisms were observed across different depth horizons. In
531 particular, higher abundances of mixotrophic MAGs compared to heterotrophic and autotrophic
532 MAGs were found in the shallower waters, suggesting that the dynamic pelagic environment of
533 the coastal wAP has selected microbial populations which can adapt to rapidly changing nutrient
534 availability. Metabolic profiles of the MAGs were phylum specific, indicating a strong link

535 between functional guilds and taxonomy. Our results highlight the novel genetic and metabolic
536 diversity present within Antarctic marine ecosystems and the need for future studies based on
537 cultivable microbes to better understand the distribution of phenotypic and genotypic traits.

538 **Data availability**

539 Sequence data for metagenomics reads from 48 samples, along with 137 dereplicated MAGs, can
540 be found under NCBI BioProject ID PRJNA894514. The MAGs have been deposited at GenBank
541 under the accession JAPKAB000000000- JAPKFH000000000.

542 **Author Contributions**

543 AD and JB designed the study and developed the first draft of the manuscript. AD developed the
544 iMAGine pipeline and conducted the analysis with assistance from JB. EC, RT, NE, and SD
545 collected the samples and edited the manuscript. EC conducted DNA extractions and processed
546 samples for sequencing. HD, DS, and OS contributed to the study design and writing.

547 **Acknowledgment**

548 We would like to thank the staff of Palmer Station and the crew of *ARSV Laurence Gould* for their
549 assistance. This work was funded by NSF-OPP 1846837 to JSB, NSF-OPP 1440435 to HD, and
550 NSF-OPP 2023425 to OS. JSB was partly supported by a Simons Foundation Early Career Marine
551 Microbial Ecology and Evolution fellowship. NE was funded through a SENECKT graduate
552 fellowship. This publication includes data generated at the UC San Diego IGM Genomics Center
553 utilizing an Illumina NovaSeq 6000 that was purchased with funding from a National Institutes of
554 Health SIG grant (#S10 OD026929).

555 **Reference**

556 Alonso-Sáez, L., Galand, P. E., Casamayor, E. O., Pedrós-Alió, C., and Bertilsson, S. (2010).
557 High bicarbonate assimilation in the dark by Arctic bacteria. *ISME Journal* 4, 1581–1590.
558 doi: 10.1038/ismej.2010.69.

559 Arrigo, K. R., van Dijken, G. L., and Bushinsky, S. (2008). Primary production in the Southern
560 Ocean, 1997-2006. *J Geophys Res Oceans* 113. doi: 10.1029/2007JC004551.

561 Baltar, F., and Herndl, G. J. (2019). Ideas and perspectives: Is dark carbon fixation relevant for
562 oceanic primary production estimates? *Biogeosciences* 16, 3793–3799. doi: 10.5194/bg-16-
563 3793-2019.

564 Bergauer, K., Fernandez-Guerra, A., Garcia, J. A. L., Sprenger, R. R., Stepanauskas, R.,
565 Pachiadaki, M. G., et al. (2018). Organic matter processing by microbial communities
566 throughout the Atlantic water column as revealed by metaproteomics. *Proceedings of the*
567 *National Academy of Sciences* 115, E400–E408.

568 Bowman, J. S., Amaral-Zettler, L. A., Rich, J. J., Luria, C. M., and Ducklow, H. W. (2017).
569 Bacterial community segmentation facilitates the prediction of ecosystem function along the
570 coast of the western Antarctic Peninsula. *ISME Journal* 11, 1460–1471. doi:
571 10.1038/ismej.2016.204.

572 Bowman, J. S., and Deming, J. W. (2017). Wind-driven distribution of bacteria in coastal
573 Antarctica: evidence from the Ross Sea region. *Polar Biol* 40, 25–35. doi: 10.1007/s00300-
574 016-1921-2.

575 Bowman, J. S., Kavanaugh, M. T., Doney, S. C., and Ducklow, H. W. (2018). Recurrent
576 seascape units identify key ecological processes along the western Antarctic Peninsula.
577 *Glob Chang Biol* 24, 3065–3078. doi: 10.1111/gcb.14161.

578 Bowman, J. S., van Mooy, B. A. S., Lowenstein, D. P., Fredricks, H. F., Hansel, C. M., Gast, R.,
579 et al. (2021). Whole Community Metatranscriptomes and Lipidomes Reveal Diverse
580 Responses Among Antarctic Phytoplankton to Changing Ice Conditions. *Front Mar Sci* 8.
581 doi: 10.3389/fmars.2021.593566.

582 Bowman, J. S., Vick-Majors, T. J., Morgan-Kiss, R., Takacs-Vesbach, C., Ducklow, H. W., and
583 Priscu, J. C. (2016). Microbial Community Dynamics in Two Polar Extremes: The Lakes of
584 the McMurdo Dry Valleys and the West Antarctic Peninsula Marine Ecosystem. *Bioscience*
585 66, 829–847. doi: 10.1093/biosci/biw103.

586 Buchan, A., LeCleir, G. R., Gulvik, C. A., and González, J. M. (2014). Master recyclers: features
587 and functions of bacteria associated with phytoplankton blooms. *Nat Rev Microbiol* 12,
588 686–698. doi: 10.1038/nrmicro3326.

589 Buchfink, B., Xie, C., and Huson, D. H. (2014). Fast and sensitive protein alignment using
590 DIAMOND. *Nat Methods* 12, 59–60. doi: 10.1038/nmeth.3176.

591 Bushnell, B. (2014). BBMap: a fast, accurate, splice-aware aligner. Lawrence Berkeley National
592 Lab.(LBNL), Berkeley, CA (United States).

593 Cantalapiedra, C. P., Hernández-Plaza, A., Letunic, I., Bork, P., and Huerta-Cepas, J. (2021).
594 eggNOG-mapper v2: Functional Annotation, Orthology Assignments, and Domain
595 Prediction at the Metagenomic Scale. *Mol Biol Evol* 38, 5825–5829. doi:
596 10.1093/molbev/msab293.

597 Cape, M. R., Vernet, M., Pettit, E. C., Wellner, J., Truffer, M., Akie, G., et al. (2019).
598 Circumpolar deep water impacts glacial meltwater export and coastal biogeochemical
599 cycling along the west Antarctic Peninsula. *Front Mar Sci* 6. doi:
600 10.3389/fmars.2019.00144.

601 Chaumeil, P. A., Mussig, A. J., Hugenholtz, P., and Parks, D. H. (2020). GTDB-Tk: A toolkit to
602 classify genomes with the genome taxonomy database. *Bioinformatics* 36, 1925–1927. doi:
603 10.1093/bioinformatics/btz848.

604 Chen, S., Zhou, Y., Chen, Y., and Gu, J. (2018). Fastp: An ultra-fast all-in-one FASTQ
605 preprocessor. in *Bioinformatics* (Oxford University Press), i884–i890. doi:
606 10.1093/bioinformatics/bty560.

607 Clarke, A., Murphy, E. J., Meredith, M. P., King, J. C., Peck, L. S., Barnes, D. K. A., et al.
608 (2007). Climate change and the marine ecosystem of the western Antarctic Peninsula.
609 *Philosophical Transactions of the Royal Society B: Biological Sciences* 362, 149–166. doi:
610 10.1098/rstb.2006.1958.

611 Connelly, T. L., Baer, S. E., Cooper, J. T., Bronk, D. A., and Wawrik, B. (2014). Urea uptake
612 and carbon fixation by marine pelagic bacteria and archaea during the Arctic summer and
613 winter seasons. *Appl Environ Microbiol* 80, 6013–6022.

614 Dutta, A., Goldman, T., Keating, J., Burke, E., Williamson, N., Dirmeier, R., et al. (2022).
615 Machine Learning Predicts Biogeochemistry from Microbial Community Structure in a
616 Complex Model System. Available at: <https://journals.asm.org/journal/spectrum>.

617 Green, J. L., Bohannan, B. J. M., and Whitaker, R. J. (2008). Microbial biogeography: From
618 taxonomy to traits. *Science* (1979) 320, 1039–1043. doi: 10.1126/science.1153475.

619 Grzymski, J. J., Riesenfeld, C. S., Williams, T. J., Dussaq, A. M., Ducklow, H., Erickson, M., et
620 al. (2012). A metagenomic assessment of winter and summer bacterioplankton from
621 Antarctica Peninsula coastal surface waters. *ISME Journal* 6, 1901–1915. doi:
622 10.1038/ismej.2012.31.

623 Gurevich, A., Saveliev, V., Vyahhi, N., and Tesler, G. (2013). QUAST: quality assessment tool
624 for genome assemblies. *Bioinformatics* 29, 1072–1075.

625 Herpell, J. B., Schindler, F., Bejtović, M., Fragner, L., Diallo, B., Bellaire, A., et al. (2020). The
626 Potato Yam Phyllosphere Ectosymbiont Paraburkholderia sp. Msb3 Is a Potent Growth
627 Promotor in Tomato. *Front Microbiol* 11. doi: 10.3389/fmicb.2020.00581.

628 Huerta-Cepas, J., Szklarczyk, D., Heller, D., Hernández-Plaza, A., Forsslund, S. K., Cook, H., et
629 al. (2019). EggNOG 5.0: A hierarchical, functionally and phylogenetically annotated
630 orthology resource based on 5090 organisms and 2502 viruses. *Nucleic Acids Res* 47,
631 D309–D314. doi: 10.1093/nar/gky1085.

632 Hyatt, D., Chen, G.-L., Locascio, P. F., Land, M. L., Larimer, F. W., and Hauser, L. J. (2010).
633 Prodigal: prokaryotic gene recognition and translation initiation site identification.
634 Available at: <http://www.biomedcentral.com/1471-2105/11/119>.

635 Kanehisa, M., Sato, Y., and Morishima, K. (2016). BlastKOALA and GhostKOALA: KEGG
636 Tools for Functional Characterization of Genome and Metagenome Sequences. *J Mol Biol*
637 428, 726–731. doi: 10.1016/j.jmb.2015.11.006.

638 Kang, D. D., Li, F., Kirton, E., Thomas, A., Egan, R., An, H., et al. (2019). MetaBAT 2: an
639 adaptive binning algorithm for robust and efficient genome reconstruction from
640 metagenome assemblies. *PeerJ* 7, e7359–e7359. doi: 10.7717/peerj.7359.

641 Kolde, R. (2019). Package ‘pheatmap.’ Available at: <https://cran.r-project.org/web/packages/pheatmap/pheatmap.pdf>.

643 Kozlov, A. M., Darriba, D., Flouri, T., Morel, B., and Stamatakis, A. (2019). RAxML-NG: A
644 fast, scalable and user-friendly tool for maximum likelihood phylogenetic inference.
645 *Bioinformatics* 35, 4453–4455. doi: 10.1093/bioinformatics/btz305.

646 Land, M., Hauser, L., Jun, S. R., Nookaew, I., Leuze, M. R., Ahn, T. H., et al. (2015). Insights
647 from 20 years of bacterial genome sequencing. *Funct Integr Genomics* 15, 141–161. doi:
648 10.1007/s10142-015-0433-4.

649 Lappan, R., Shelley, G., Islam, Z. F., Leung, P. M., Lockwood, S., Nauer, P. A., et al. (2023).
650 Molecular hydrogen in seawater supports growth of diverse marine bacteria. *Nat Microbiol.*
651 doi: 10.1038/s41564-023-01322-0.

652 Li, H. (2013). Aligning sequence reads, clone sequences and assembly contigs with BWA-MEM.
653 Available at: <http://arxiv.org/abs/1303.3997>.

654 Li, H., Handsaker, B., Wysoker, A., Fennell, T., Ruan, J., Homer, N., et al. (2009). The Sequence
655 Alignment/Map format and SAMtools. *Bioinformatics* 25, 2078–2079. doi:
656 10.1093/bioinformatics/btp352.

657 Lin, Y., Moreno, C., Marchetti, A., Ducklow, H., Schofield, O., Delage, E., et al. (2021). Decline
658 in plankton diversity and carbon flux with reduced sea ice extent along the Western
659 Antarctic Peninsula. *Nat Commun* 12. doi: 10.1038/s41467-021-25235-w.

660 Loy, A., Duller, S., Baranyi, C., Mußmann, M., Ott, J., Sharon, I., et al. (2009). Reverse
661 dissimilatory sulfite reductase as phylogenetic marker for a subgroup of sulfur-oxidizing
662 prokaryotes. *Environ Microbiol* 11, 289–299. doi: 10.1111/j.1462-2920.2008.01760.x.

663 Malard, L. A., Avila-Jimenez, M. L., Schmale, J., Cuthbertson, L., Cockerton, L., and Pearce, D.
664 A. (2022). Aerobiology over the Southern Ocean – Implications for bacterial colonization of
665 Antarctica. *Environ Int* 169. doi: 10.1016/j.envint.2022.107492.

666 McLeod, D. J., Hallegraeff, G. M., Hosie, G. W., and Richardson, A. J. (2012). Climate-driven
667 range expansion of the red-tide dinoflagellate *Noctiluca scintillans* into the Southern Ocean.
668 *J Plankton Res* 34, 332–337. doi: 10.1093/plankt/fbr112.

669 McMurdie, P. J., and Holmes, S. (2013). phyloseq: an R package for reproducible interactive
670 analysis and graphics of microbiome census data. *PLoS One* 8, e61217.

671 Meredith, M. P., and King, J. C. (2005). Rapid climate change in the ocean west of the Antarctic
672 Peninsula during the second half of the 20th century. *Geophys Res Lett* 32, 1–5. doi:
673 10.1029/2005GL024042.

674 Murphy, C. L., Yang, R., Decker, T., Cavalliere, C., Andreev, V., Bircher, N., et al. (2021).
675 Genomes of novel myxococcota reveal severely curtailed machineries for predation and
676 cellular differentiation. *Appl Environ Microbiol* 87. doi: 10.1128/AEM.01706-21.

677 Nurk, S., Meleshko, D., Korobeynikov, A., and Pevzner, P. A. (2017). metaSPAdes: a new
678 versatile metagenomic assembler. *Genome Res* 27, 824–834.

679 Oijen, T. van Leeuwe, M. A. van, and Gieskes, W. W. C. (2003). Variation of particulate
680 carbohydrate pools over time and depth in a diatom-dominated plankton community at the
681 Antarctic Polar Front. *Polar Biol* 26, 195–201. doi: 10.1007/s00300-002-0456-x.

682 Oksanen, J., Kindt, R., Legendre, P., O'Hara, B., Stevens, M. H. H., Oksanen, M. J., et al.
683 (2007). The vegan package. *Community ecology package* 10, 631–637.

684 Olm, M. R., Brown, C. T., Brooks, B., and Banfield, J. F. (2017). DRep: A tool for fast and
685 accurate genomic comparisons that enables improved genome recovery from metagenomes
686 through de-replication. *ISME Journal* 11, 2864–2868. doi: 10.1038/ismej.2017.126.

687 Parks, D. H., Imelfort, M., Skennerton, C. T., Hugenholtz, P., and Tyson, G. W. (2015).
688 CheckM: assessing the quality of microbial genomes recovered from isolates, single cells,
689 and metagenomes. *Genome Res* 25, 1043–1055.

690 Parks, D. H., Rinke, C., Chuvochina, M., Chaumeil, P. A., Woodcroft, B. J., Evans, P. N., et al.
691 (2017). Recovery of nearly 8,000 metagenome-assembled genomes substantially expands
692 the tree of life. *Nat Microbiol* 2, 1533–1542. doi: 10.1038/s41564-017-0012-7.

693 Plum, C., Hillebrand, H., and Moorthi, S. (2020). Krill vs salps: dominance shift from krill to
694 salps is associated with higher dissolved N:P ratios. *Sci Rep* 10, 5911. doi: 10.1038/s41598-
695 020-62829-8.

696 Royo-Llonch, M., Sánchez, P., Ruiz-González, C., Salazar, G., Pedrós-Alió, C., Sebastián, M., et
697 al. (2021). Compendium of 530 metagenome-assembled bacterial and archaeal genomes
698 from the polar Arctic Ocean. *Nat Microbiol* 6, 1561–1574. doi: 10.1038/s41564-021-00979-
699 9.

700 Saba, G. K., Fraser, W. R., Saba, V. S., Iannuzzi, R. A., Coleman, K. E., Doney, S. C., et al.
701 (2014). Winter and spring controls on the summer food web of the coastal West Antarctic
702 Peninsula. *Nat Commun* 5. doi: 10.1038/ncomms5318.

703 Schofield, O., Brown, M., Kohut, J., Nardelli, S., Saba, G., Waite, N., et al. (2018). Changes in
704 the upper ocean mixed layer and phytoplankton productivity along the West Antarctic
705 Peninsula. *Philosophical Transactions of the Royal Society A: Mathematical, Physical and*
706 *Engineering Sciences* 376. doi: 10.1098/rsta.2017.0173.

707 Seyitmuhammedov, K., Stirling, C. H., Reid, M. R., van Hale, R., Laan, P., Arrigo, K. R., et al.
708 (2022). The distribution of Fe across the shelf of the Western Antarctic Peninsula at the start
709 of the phytoplankton growing season. *Mar Chem* 238. doi:
710 10.1016/j.marchem.2021.104066.

711 Shaffer, M., Borton, M. A., McGivern, B. B., Zayed, A. A., la Rosa, S. L. 0003 3527 8101,
712 Soden, L. M., et al. (2020). DRAM for distilling microbial metabolism to automate the
713 curation of microbiome function. *Nucleic Acids Res* 48, 8883–8900. doi:
714 10.1093/nar/gkaa621.

715 Siegert, M., Atkinson, A., Banwell, A., Brandon, M., Convey, P., Davies, B., et al. (2019). The
716 Antarctic Peninsula under a 1.5°C global warming scenario. *Front Environ Sci* 7. doi:
717 10.3389/fenvs.2019.00102.

718 Sriswasdi, S., Yang, C. C., and Iwasaki, W. (2017). Generalist species drive microbial dispersion
719 and evolution. *Nat Commun* 8. doi: 10.1038/s41467-017-01265-1.

720 Team, Rs. (2015). RStudio: integrated development for R. *RStudio, Inc., Boston, MA URL*
721 <http://www.rstudio.com> 42, 84.

722 Thompson, L. R., Sanders, J. G., McDonald, D., Amir, A., Ladau, J., Locey, K. J., et al. (2017).
723 A communal catalogue reveals Earth's multiscale microbial diversity. *Nature* 551, 457–463.
724 doi: 10.1038/nature24621.

725 Wang, K., Wu, Y., Ye, M., Yang, Y., Asiegbu, F. O., Overmyer, K., et al. (2021). Comparative
726 Genomics Reveals Potential Mechanisms of Plant Beneficial Effects of a Novel Bamboo-
727 Endophytic Bacterial Isolate Paraburkholderia sacchari Suichang626. *Front Microbiol* 12.
728 doi: 10.3389/fmicb.2021.686998.

729 Waters, K. J., and Smith, R. C. (1992). Palmer LTER: A sampling grid for the Palmer LTER
730 program. *Antarct J US* 27, 236–239.

731 Williams, T. J., Long, E., Evans, F., Demaere, M. Z., Lauro, F. M., Raftery, M. J., et al. (2012).
732 A metaproteomic assessment of winter and summer bacterioplankton from Antarctic
733 Peninsula coastal surface waters. *ISME Journal* 6, 1883–1900. doi: 10.1038/ismej.2012.28.

734 Yu, Y., Liu, X., Miao, J., and Leng, K. (2020). Chitin from Antarctic krill shell: Eco-preparation,
735 detection, and characterization. *Int J Biol Macromol* 164, 4125–4137. doi:
736 10.1016/j.ijbiomac.2020.08.244.

737

738

739 **Figure Legend**

740 **Figure 1:** Sample locations in the western Antarctic Peninsula. S - only shallower samples
741 analyzed, M- only medium-depth samples analyzed, D - only deeper samples analyzed, S-M-D –
742 samples collected from deep, medium, and shallow environments analyzed.

743 **Figure 2:** Principal coordinates analysis (PCoA) of Bray-Curtis dissimilarity based on normalized
744 gene coverage across 48 samples. Symbol shape and color indicates sample region and depth,
745 respectively.

746 **Figure 3:** Boxplot showing the distribution of different carbon cycle genes related to (A) carbon
747 fixation, (B) CO oxidation, (C) fermentation, and (D) methane oxidation across different depth
748 horizons of the WAP. Normalized coverages of genes grouped in each of these categories are listed
749 in Supplementary Figure S1. A pairwise comparison for significance was conducted using the
750 Wilcoxon test.

751 **Figure 4:** Boxplot showing the distribution of different sulfur cycle genes related to (A) sulfur
752 oxidation, (B) dissimilatory sulfate reduction, and (C) thiosulfate to sulfide reduction across
753 different depth horizons of the WAP. Normalized coverages of genes grouped in each of these
754 categories are listed in Supplementary Figure S2. A pairwise comparison for significance was
755 conducted using the Wilcoxon test.

756 **Figure 5:** Boxplot showing the distribution of different nitrogen cycle genes related to (A)
757 nitrification, (B) denitrification, (C) dissimilatory nitrate reduction to ammonia (DNRA), and (D)
758 urea utilization across different depth horizons of the WAP. Normalized coverages of genes
759 grouped in each of these categories are listed in Supplementary Figure S3. A pairwise comparison
760 for significance was conducted using the Wilcoxon test.

761 **Figure 6:** Boxplot showing the distribution of different carbohydrate transformation genes related
762 to (A) cellulose, (B) pectin RGI, (C) starch, (D) xyloglucan, and (E) chitin degradation across
763 different depth horizons of the WAP. Normalized coverages of genes grouped in each of these
764 categories are listed in Supplementary Figure S4. A pairwise comparison for significance was
765 conducted using the Wilcoxon test.

766 **Figure 7:** rage abundance of 137 dereplicated MAGs across (A) Shallow, (B) Medium, and
767 (C) Deep Waters of the coastal wAP. Each dereplicated MAG represents multiple MAGs from
768 different samples. The average abundance of each dereplicated MAG represents the average
769 abundance of all the MAGs it represents from a particular depth horizon.

770 **Figure 8:** Maximum-likelihood phylogenomic analysis of 137 dereplicated MAGs based on (A)
771 archaeal and (B) bacterial marker genes from GTDB-Tk analysis. Detailed genome statistics and
772 taxonomy are provided in Supplementary Table S3, and the detailed pathways and functions are
773 provided in Supplementary Table S4. Phylum, completeness %, contamination %, and bootstrap
774 legends are domain-specific, whereas depth, region, and function are common for bacteria and
775 archaea. Depth (represented by a star) and region (represented by a right triangle)
776 symbols are present on the terminal node and terminal branch, respectively. The circle symbols
777 in the outermost layer depict the functional capabilities of each MAG. All the carbohydrates
778 mentioned represent the presence of enzymes capable of degrading them. Xylan and/or xyloglucan
779 degrading enzymes are represented by hemicellulose in this figure. The hyphenated legends for
780 depth represent MAGs found in multiple depth horizons, whereas hyphenated legends for regions
781 represent MAGs found in multiple regions.

782 **Figure 9:** Non-Metric Multidimensional Scaling (NMDS) of binary matrix based on the presence
783 or absence of genes predicted by Ghost Koala across 127 dereplicated bacterial MAGs.
784 Abbreviations of metabolic categories as used in the CAP analysis are as follows: GU: Glucose

785 utilization; CF: carbon fixing pathways; NI: nitrification; SO: sulfur oxidation; DNR –
786 Denitrification; DSR – Dissimilatory sulfite reduction.

787 **Figure 10:** Comparison of MAGs having different metabolic lifestyles (A) Venn Diagram
788 showing overlaps among different metabolic categories of the MAGs. GU: Glucose utilization;
789 CF: carbon fixing pathways; NI: nitrification; SO: sulfur oxidation.  Boxplot showing genome
790 sizes of MAGs related to different metabolic lifestyles. The details of the genome sizes and
791 metabolic lifestyle of each MAG are reported in Supplementary Table 3.  Boxplot showing
792 mapped read percentage of MAGs having different metabolic lifestyles in shallower depth
793 samples. For the boxplots, a pairwise comparison for significance was conducted using the
794 Wilcoxon test.

795

796 **Supplementary Table Legend**

797 **Table S1:** Sample metadata for 48 samples

798 **Table S2:** Detailed genome statistics of 137 MAGs

799 **Table S3:** Detailed taxonomic classification-based genome summary

800 **Table S4:** Metabolic profiles of 137 MAGs

801

